GPH-International Journal of Applied Science
(Online ISSN 3050-9653)
Volume 09 | Issue 01 | 2026
Published by: Global Publication House
DOI: https://doi.org/10.5281/zenodo.21396358
Available online at: www.gphjournal.org
Journal homepage: https://gphjournal.org/index.php/as/index

Magnetohydrodynamic (MHD) Unsteady Axial Flow in an Annulus: A semi-analytical Approach

Jibrin Danjuma Yahaya[1], Agbata Benedict Celestine[1], Raji Muhammed[1], Abraham Ayegba Alfa[2], Jacob Funsho Omonile[3], Joshua Attah[4]
[1]*Department of Mathematics and Statistics, Confluence University of Science and Technology, Osara, Kogi State, Nigeria.*
[2]*Department of Computer Science, Confluence University of Science and Technology, Osara, Kogi State, Nigeria.*
[3]*Department of Physics, Confluence University of Science and Technology, Osara, Kogi State, Nigeria.*
[4]*Department of Information Technology, Confluence University of Science and Technology, Osara, Kogi State, Nigeria.*
Corresponding Author: Jibrin Danjuma Yahaya; E-mail: yahayajd@custech.edu.ng

Abstract

This study presents a semi-analytical investigation of unsteady magnetohydrodynamic axial flow of an incompressible, viscous, electrically conducting Newtonian fluid through an annulus bounded by two stationary concentric cylinders. The flow is driven by a constant axial pressure gradient and subjected to a uniform transverse magnetic field. Under the low-magnetic-Reynolds-number approximation, the induced magnetic field is neglected and the Lorentz-force term appears as a linear resistance to the axial motion. The governing momentum equation is non-dimensionalized in terms of the radius ratio, dimensionless time, and Hartmann number. The resulting initial-boundary-value problem is solved using the Laplace transform method, while the Riemann-sum approximation is used to recover the transient velocity and skin-friction fields. Closed-form steady-state expressions are also obtained for the velocity and wall shear stress. The results show that the velocity increases with time and approaches the steady-state profile, while increasing the Hartmann number suppresses the axial velocity and reduces the wall shear magnitude. The transient skin friction on both annular walls approaches the corresponding steady-state value as time increases. The formulation provides a useful semi-analytical description of hydromagnetic start-up flow in annular geometries.

Keywords:

Magnetohydrodynamics; transient axial flow; Hartmann number; Laplace transform; Riemann-sum approximation; skin friction; annular flow.

Nomenclature

Symbols	Name/Unit(s)	Dimension
r':	Radial coordinate (m)	(L)
z:	Axial coordinate (m)	(L)

t:	Dimensional time (s)	(T)
r_1:	Radius of the inner cylinder (m)	(L)
r_2:	Radius of the outer cylinder (m)	(L)
$v(r', t)$:	Dimensional axial velocity (m/s)	LT^{-1}
r:	Dimensionless Radial coordinate, $\left(r = \frac{r'}{r_2}\right)$	
T:	Dimensionless time	
$V(r, T)$:	Dimensionless axial velocity	
$V_s(r)$:	Dimensionless steady-state axial velocity	
p:	Fluid pressure	$ML^{-1}T^{-2}$
$\mathcal{G}$:	Constant axial pressure gradient $ML^{-2}T^{-2}$	
ρ:	Fluid density	ML^{-3}
μ:	Dynamic viscosity	$ML^{-1}T^{-1}$
ν:	Kinematic viscosity	L^2T^{-1}
σ:	Electrical conductivity of the fluid	$M^{-1}L^{-3}T^3I^2$
B_0:	Applied magnetic field strength $MT^{-2}I^{-1}$	
λ:	Dimensionless radius ratio $\left(\lambda = \frac{r_1}{r_2}\right)$	
M:	Hartmann number	
$\mathcal{S}$:	Laplace transform parameter	
$\bar{V}(r, \mathcal{S})$:	Laplace transform of the dimensionless velocity	
$I_0(.)$:	Modified Bessel function of the first kind of order zero	
$K_0(.)$:	Modified Bessel function of the second kind of order zero	
$I_1(.)$:	Modified Bessel function of the first kind of order one	
$K_1(.)$:	Modified Bessel function of the second kind of order one	

1 Introduction

Transport phenomena in annular passages are important in fluid mechanics because annular geometries occur in several internal-flow configurations, including heat exchangers, drilling and wellbore systems, journal-bearing arrangements, rotating-cylinder devices, and electromagnetic flow-control systems. In such configurations, the presence of two cylindrical walls imposes strong geometric confinement, while the radial curvature of the annular domain modifies the diffusion of axial momentum. Unlike plane channel flow, the radial diffusion operator in an annulus contains the curvature term $(1/r)(\partial V/\partial r)$, which affects the shape of the velocity distribution and the wall shear stresses.

Unsteady annular flows have received considerable attention because the transient development of velocity and wall shear determines the start-up response, flow-rate evolution, and approach to steady motion. Semi-analytical studies of transient Dean flow and annular flow have shown that the Laplace transform method, combined with numerical inversion, is effective for resolving the development of time-dependent velocity fields in cylindrical geometries

[1], [2]. Related studies on generalized Taylor-Couette flow have also demonstrated that annular geometry, wall motion, and transient diffusion strongly influence velocity formation and shear distribution [3], [4]. Classical investigations of Taylor-Couette and axial annular flows further show that radius ratio and wall confinement significantly affect the flow structure and stability characteristics [5], [6]. Exact and limiting solutions for oscillatory pipe and annular flows provide additional analytical benchmarks for time-dependent cylindrical transport problems [7].

Recent developments have extended the analysis of unsteady cylindrical flows to more complex fluid and boundary conditions. These include dusty-fluid effects in oscillating cylindrical systems [8], variable-viscosity effects in unsteady Couette flow [9], and slip-modified magnetohydrodynamic Dean flows [10]. Such studies emphasize the continued relevance of semi-analytical methods for transient internal flows, particularly when the time-domain inversion of the transformed solution is not straightforward.

Magnetohydrodynamic flow introduces an additional resistance mechanism through the interaction between the motion of an electrically conducting fluid and an applied magnetic field. When the magnetic Reynolds number is small, the induced magnetic field may be neglected, and the electromagnetic effect enters the axial momentum equation through a Lorentz-force term proportional to the velocity. This term generally opposes the fluid motion and acts as a magnetic damping mechanism. MHD effects have been studied in Taylor-Couette and annular configurations, where the magnetic field modifies the velocity distribution, shear stress, and hydromagnetic stability characteristics [11], [12]. Related investigations of transient MHD Couette, Poiseuille, and annular flows have also shown that the Hartmann number is a principal parameter controlling the damping of conducting-fluid motion [13], [14], [15], [16].

Although many studies have considered unsteady annular flows and MHD channel flows, there remains a need for compact semi-analytical solutions for pressure-driven MHD start-up flow in annular geometries with stationary cylindrical walls. The present study addresses this problem by considering the transient axial motion of an electrically conducting Newtonian fluid in an annulus under a uniform transverse magnetic field. The governing equation is formulated under the assumptions of incompressibility, full development, axisymmetry, constant fluid properties, negligible induced magnetic field, and no slip at both cylinder walls. The Laplace transform method is used to obtain the velocity field in the transform domain, and the Riemann-sum approximation is employed to recover the transient solution. Steady-state velocity and skin-friction expressions are also derived to assess the large-time behaviour of the transient solution.

2 Physical Interpretation and Basic Equations

Consider the unsteady, fully developed, pressure-driven axial flow of an incompressible, viscous, electrically conducting Newtonian fluid through the annular region between two fixed concentric cylinders. Let r_1 and r_2 denote the radii of the inner and outer cylinders, respectively, with $0 < r_1 < r_2$. The dimensional radial coordinate is denoted by r', and the fluid occupies the annular region $r_1 \leq r' \leq r_2$. The flow is assumed to be axisymmetric and fully developed in the axial direction. Hence, the velocity field has only an axial component, $\mathbf{V} = (0,0, v(r', t))$, where $v(r', t)$ is the dimensional axial velocity and t is time. The cylinders are stationary, and the no-slip condition is imposed at both annular walls. The flow is driven by a constant axial pressure gradient, while a uniform transverse magnetic field of strength B_0 is applied to the electrically conducting fluid. The magnetic Reynolds number is assumed to be sufficiently small so that the induced magnetic field is neglected. Under this approximation, the magnetic contribution appears as a Lorentz-force resistance proportional to the velocity.

Physically, the axial pressure gradient drives the fluid motion, viscosity diffuses axial momentum across the annular gap, and the Lorentz force opposes the motion of the conducting fluid. The transient flow field is therefore governed by the balance among pressure forcing, viscous diffusion, magnetic damping, and wall confinement. The model geometry of the flow is given in Figure 1 below:

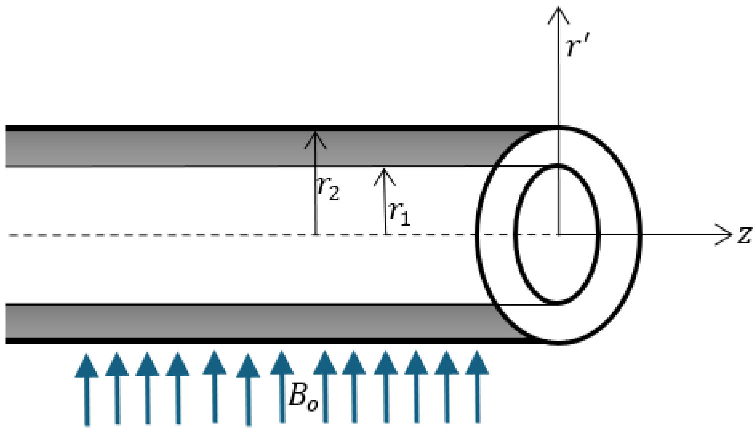

Figure 1: Schematic of the flow physics

2.1 Dimensional governing equations

For the assumed unidirectional axial flow, the continuity equation is automatically satisfied. The axial momentum equation in cylindrical coordinates is:

$$\rho\frac{\partial v}{\partial t} = -\frac{\partial p}{\partial z} + \mu\left(\frac{\partial^2 v}{\partial r'^2} + \frac{1}{r'}\frac{\partial v}{\partial r'}\right) - \sigma B_0^2 v, \tag{1}$$

Where ρ is the fluid density, μ is the dynamic viscosity, σ is the electrical conductivity, B_0 is the magnetic-field strength, and p is the pressure. Let the imposed pressure gradient be constant and defined by $-\frac{\partial p}{\partial z} = \mathcal{G}, \mathcal{G} > 0$. Then the dimensional governing equation becomes:

$$\rho\frac{\partial v}{\partial t} = \mathcal{G} + \mu\left(\frac{\partial^2 v}{\partial r'^2} + \frac{1}{r'}\frac{\partial v}{\partial r'}\right) - \sigma B_0^2 v. \tag{2}$$

The initial and the no-slip boundary conditions are:

$$v(r', 0) = 0, r_1 \leq r' \leq r_2. \tag{3}$$

$$v(r_1, t) = 0, v(r_2, t) = 0, t > 0, \tag{4}$$

The dimensional skin frictions are:

$$\tau_{r_1} = \mu\frac{\partial v}{\partial r'}\bigg|_{r'=r_1}, \tau_{r_2} = \mu\frac{\partial v}{\partial r'}\bigg|_{r'=r_2}. \tag{5}$$

2.2 Dimensionless governing equations

Introduce the dimensionless variables:

$$r = \frac{r'}{r_2}, \lambda = \frac{r_1}{r_2}, T = \frac{\nu t}{r_2^2}, V(r, T) = \frac{\mu v(r', t)}{\mathcal{G} r_2^2}, \nu = \frac{\mu}{\rho}, M^2 = \frac{\sigma B_0^2 r_2^2}{\mu}. \tag{6}$$

ν is the kinematic viscosity, and λ is the radius ratio, M is the Hartmann number. The annular domain becomes, $\lambda \leq r \leq 1$.

Using these definitions, the non-dimensional governing equation becomes:

$$\frac{\partial V}{\partial T} = \frac{\partial^2 V}{\partial r^2} + \frac{1}{r}\frac{\partial V}{\partial r} - (\mathcal{S} + M^2)V + 1. \tag{7}$$

The dimensionless initial boundary conditions are:

$$V(r,0) = 0, \lambda \leq r \leq 1, \tag{8}$$

$$V(\lambda,T) = 0, V(1,T) = 0, T > 0. \tag{9}$$

The parameter M measures the strength of magnetic damping relative to viscous diffusion. When $M = 0$, the problem reduces to the classical start-up pressure-driven annular flow without magnetic damping. For $M > 0$, the Lorentz-force term $-M^2V$ suppresses the axial motion.

3 Solution

The dimensionless problem is solved using the Laplace transform in time. Let the Laplace transform of function as defined in the work of [17] be

$$\bar{V}(r,\mathcal{S}) = \mathcal{L}\{V(r,T)\} = \int_0^\infty e^{-\mathcal{S}T}\, V(r,T)\, dT. \tag{10}$$

Applying the Laplace transform to equations (7) - (9) and simplifications, we obtain:

$$\frac{d^2\bar{V}}{dr^2} + \frac{1}{r}\frac{d\bar{V}}{dr} - (\mathcal{S} + M^2)\bar{V} = -\frac{1}{\mathcal{S}}, \tag{11}$$

$$\bar{V}(\lambda,\mathcal{S}) = 0, \bar{V}(1,\mathcal{S}) = 0. \tag{12}$$

The associated homogeneous equation is a modified Bessel equation of order zero. Therefore, the transformed solution has the form:

$$\bar{V}(r,\mathcal{S}) = C_1 I_0(r\sqrt{\mathcal{S} + M^2}) + C_2 K_0(r\sqrt{\mathcal{S} + M^2}) + \frac{1}{\mathcal{S}(\mathcal{S}+M^2)}, \tag{13}$$

where I_0 and K_0 are modified Bessel functions of the first and second kinds of order zero and C_1 and C_2, are obtained as:

$$C_1 = \frac{K_0(\sqrt{\mathcal{S} + M^2}) - K_0(\lambda\sqrt{\mathcal{S} + M^2})}{\mathcal{S}(\mathcal{S} + M^2)\left[I_0\left(\sqrt{\mathcal{S} + M^2}\right)K_0\left(\lambda\sqrt{\mathcal{S} + M^2}\right) - I_0\left(\lambda\sqrt{\mathcal{S} + M^2}\right)K_0\left(\sqrt{\mathcal{S} + M^2}\right)\right]},$$

and

$$C_2 = \frac{I_0(\lambda\sqrt{\mathcal{S}+M^2}) - I_0(\sqrt{\mathcal{S}+M^2})}{\mathcal{S}(\mathcal{S}+M^2)\left[I_0\left(\sqrt{\mathcal{S}+M^2}\right)K_0\left(\lambda\sqrt{\mathcal{S}+M^2}\right) - I_0\left(\lambda\sqrt{\mathcal{S}+M^2}\right)K_0\left(\sqrt{\mathcal{S}+M^2}\right)\right]}.$$

3.1 Velocity profile

The velocity profile is obtained in two forms: the transient velocity profile in the Laplace domain and the steady-state velocity profile in closed form.

3.1.1 Unsteady velocity profile

Substitution of the constants C_1 and C_2 into the transformed velocity field (13) gives:

$$\bar{V}(r,\mathcal{S}) = \frac{1}{\mathcal{S}(\mathcal{S}+M^2)}\left[1 + \frac{\left\{K_0\left(\sqrt{\mathcal{S}+M^2}\right) - K_0\left(\lambda\sqrt{\mathcal{S}+M^2}\right)\right\}I_0\left(r\sqrt{\mathcal{S}+M^2}\right) + \left\{I_0\left(\lambda\sqrt{\mathcal{S}+M^2}\right) - I_0\left(\sqrt{\mathcal{S}+M^2}\right)\right\}K_0\left(r\sqrt{\mathcal{S}+M^2}\right)}{I_0\left(\sqrt{\mathcal{S}+M^2}\right)K_0\left(\lambda\sqrt{\mathcal{S}+M^2}\right) - I_0\left(\lambda\sqrt{\mathcal{S}+M^2}\right)K_0\left(\sqrt{\mathcal{S}+M^2}\right)}\right] \quad (14)$$

The corresponding time-domain velocity is formally

$$V(r,T) = \mathcal{L}^{-1}\{\bar{V}(r,\mathcal{S})\}. \quad (15)$$

Since the transformed solution contains modified Bessel functions with complex Laplace parameter $\mathcal{S}$, direct analytical inversion is generally not convenient. Therefore, the Riemann-sum approximation method is employed to numerically recover the transient solution.

3.1.2 Steady velocity profile

At steady state, $\frac{\partial V}{\partial T} = 0$. Therefore, equation (8) is reduced to:

$$\frac{d^2V_s}{dr^2} + \frac{1}{r}\frac{dV_s}{dr} - M^2V_s = -1. \quad (16)$$

The steady solution is:

$$V_s(r) = C_3I_0(rM) + C_4K_0(rM) + \frac{1}{M^2}. \quad (17)$$

Using

$$V_s(\lambda) = 0, V_s(1) = 0, \quad (18)$$

we obtain:

$$C_3 = \frac{K_0(M) - K_0(\lambda M)}{M^2[I_0(M)K_0(\lambda M) - I_0(\lambda M)K_0(M)]},$$

and

$$C_4 = \frac{I_0(\lambda M) - I_0(M)}{M^2[I_0(M)K_0(\lambda M) - I_0(\lambda M)K_0(M)]}.$$

respectively.

Thus, the steady velocity profile is:

$$V_s(r) = \frac{1}{M^2}\left[1+\frac{\{K_0(M)-K_0(\lambda M)\}I_0(rM)+\{I_0(\lambda M)-I_0(M)\}K_0(rM)}{I_0(M)K_0(\lambda M)-I_0(\lambda M)K_0(M)}\right]. \quad (19)$$

This expression represents the limiting velocity distribution approached by the transient solution as $T \to \infty$.

3.2 Skin friction

The dimensionless skin friction is proportional to the radial derivative of the dimensionless velocity. Define by: $C_f(r,T) = \frac{\partial V}{\partial r}$.

The inner-wall and outer-wall skin frictions are respectively $C_{f,\lambda}(T) = \left.\frac{\partial V}{\partial r}\right|_{r=\lambda}$, and $C_{f,1}(T) = \left.\frac{\partial V}{\partial r}\right|_{r=1}$. Because the velocity satisfies the no-slip condition at both walls, these quantities measure the shear response of the annular boundaries.

3.2.1 Unsteady skin friction

In the Laplace domain,

$$\bar{C}_{f,\lambda}(\mathcal{S}) = \left[\frac{\{K_0(\sqrt{\mathcal{S}+M^2})-K_0(\lambda\sqrt{\mathcal{S}+M^2})\}I_1(\lambda\sqrt{\mathcal{S}+M^2})-\{I_0(\lambda\sqrt{\mathcal{S}+M^2})-I_0(\sqrt{\mathcal{S}+M^2})\}K_1(\lambda\sqrt{\mathcal{S}+M^2})}{\mathcal{S}(\sqrt{\mathcal{S}+M^2})[I_0(\sqrt{\mathcal{S}+M^2})K_0(\lambda\sqrt{\mathcal{S}+M^2})-I_0(\lambda\sqrt{\mathcal{S}+M^2})K_0(\sqrt{\mathcal{S}+M^2})]}\right]. \quad (20)$$

and

$$\bar{C}_{f,1}(\mathcal{S}) = \left[\frac{\{K_0(\sqrt{\mathcal{S}+M^2})-K_0(\lambda\sqrt{\mathcal{S}+M^2})\}I_1(\sqrt{\mathcal{S}+M^2})-\{I_0(\lambda\sqrt{\mathcal{S}+M^2})-I_0(\sqrt{\mathcal{S}+M^2})\}K_1(\sqrt{\mathcal{S}+M^2})}{\mathcal{S}(\sqrt{\mathcal{S}+M^2})[I_0(\sqrt{\mathcal{S}+M^2})K_0(\lambda\sqrt{\mathcal{S}+M^2})-I_0(\lambda\sqrt{\mathcal{S}+M^2})K_0(\sqrt{\mathcal{S}+M^2})]}\right]. \quad (21)$$

The time-domain unsteady skin frictions are obtained through inverse Laplace transformation:

$$C_{f,\lambda}(T) = \mathcal{L}^{-1}\{\bar{C}_{f,\lambda}(\mathcal{S})\}, \quad (22)$$

$$C_{f,1}(T) = \mathcal{L}^{-1}\{\bar{C}_{f,1}(\mathcal{S})\}. \quad (23)$$

3.2.2 Steady skin friction

Using the steady velocity of equation (17), the steady skin friction at the inner and outer cylinders is:

$$C_{f,\lambda}^{(st)} = \frac{[K_0(M)-K_0(\lambda M)]I_1(\lambda M)-[I_0(\lambda M)-I_0(M)]K_1(\lambda M)}{M[I_0(M)K_0(\lambda M)-I_0(\lambda M)K_0(M)]}, \quad (24)$$

$$C_{f,1}^{(st)} = \frac{[K_0(M)-K_0(\lambda M)]I_1(M)-[I_0(\lambda M)-I_0(M)]K_1(M)}{M[I_0(M)K_0(\lambda M)-I_0(\lambda M)K_0(M)]}. \tag{25}$$

These steady expressions provide reference values for assessing the large-time behaviour of the transient skin-friction solution.

3.3 Riemann-sum Approximation of Laplace Inversion

The Laplace-domain velocity and skin-friction expressions contain modified Bessel functions with the complex Laplace parameter. Although the transformed solution is available in closed form, direct analytical inversion is generally not convenient. Therefore, the transient velocity and wall shear stresses are recovered numerically using the Riemann-sum approximation for Laplace inversion. This approach has been used in related transient annular and Dean-flow studies because it allows the time-dependent solution to be obtained from the transformed expression without direct time marching [17], [18].

Let $\bar{F}(\mathcal{S})$ be the Laplace transform of a time-dependent function $F(T)$. The inverse transform is approximated by

$$F(T,r) = \frac{e^{\epsilon T}}{T}\left[\frac{1}{2}\bar{F}(\epsilon,r) + \mathrm{Re}\sum_{k=1}^{N} \bar{F}\left(\epsilon + \frac{ik\pi}{T},r\right)(-1)^k\right], \tag{26}$$

where $i = \sqrt{-1}, N$ is the number of terms retained in the finite summation, and ϵ is a positive convergence parameter. The value of N is chosen sufficiently large to ensure stable numerical convergence. In practical computations, $\epsilon T \approx 4.7$ is commonly used as a convergence criterion, although the optimal choice may depend on the required accuracy and the range of dimensionless time.

For the present problem, Eq. (26) is applied separately to the transformed velocity $\bar{V}(r,\mathcal{S})$, the inner-wall transformed skin friction $\bar{C}_{f,\lambda}(\mathcal{S})$, and the outer-wall transformed skin friction $\bar{C}_{f,1}(\mathcal{S})$. Thus,

$$V(r,T) = \mathcal{L}^{-1}\{\bar{V}(r,\mathcal{S})\},$$
$$C_{f,\lambda}(T) = \mathcal{L}^{-1}\{\bar{C}_{f,\lambda}(\mathcal{S})\},$$
$$C_{f,1}(T) = \mathcal{L}^{-1}\{\bar{C}_{f,1}(\mathcal{S})\}.$$

The large-time behaviour of the Riemann-sum solution is assessed by comparing the transient results with the corresponding steady-state velocity and skin-friction expressions. This comparison is important because the unsteady solution must approach the steady solution as $T \to \infty$.

4 Results and Discussion

The numerical results describe the transient development of MHD pressure-driven axial flow in a stationary annulus. The main governing parameters are the dimensionless time T, Hartmann number M, and radius ratio λ. The Hartmann number appears in the governing equation through the damping term $-M^2V$, which represents the Lorentz-force resistance opposing the axial motion. The radius ratio controls the width of the annular gap and therefore influences both the velocity distribution and the wall shear stress.

4.1 Effect of dimensionless time on velocity

Figure 2 shows the effect of dimensionless time T on the velocity profile for $M = 1.0$. At small time, the velocity is low because the fluid starts from rest and the pressure-driven motion has not fully developed across the annular gap. As T increases, the velocity increases throughout the annular region and gradually approaches a steady profile.

The velocity satisfies the no-slip condition at both walls and reaches its maximum within the annular gap. The profile is not exactly symmetric because the cylindrical diffusion operator contains the curvature term $(1/r)(\partial V/\partial r)$. This curvature effect is a characteristic feature of annular flow and distinguishes the present problem from plane channel flow.

The numerical values in Table 1 confirm the transient-to-steady development. For $M = 0.5$ at $r = 0.6$, the RSA velocity increases from 0.0780 at $T = 0.2$ to 0.0822 at $T = 0.4$, and then reaches the steady-state value 0.0824. For $M = 1.0$ at the same radial location, the RSA velocity increases from 0.0747 at $T = 0.2$ to 0.0782 at $T = 0.4$, approaching the steady-state value 0.0783. This agreement shows that the transient solution approaches the steady-state limit as time increases.

4.2 Effect of Hartmann number on velocity

Figure 3 presents the influence of Hartmann number on the axial velocity profile for fixed $T = 0.02$. The velocity decreases as M increases. This behaviour follows directly from the magnetic damping term $-M^2V$. A stronger magnetic field increases the Lorentz-force resistance, which suppresses the axial motion of the electrically conducting fluid.

The trend is also evident in Table 1. At $T = 0.2$ and $r = 0.6$, the RSA velocity decreases from 0.0780 for $M = 0.5$ to 0.0747 for $M = 1.0$. At steady state, the corresponding velocity decreases from 0.0824 to 0.0783. Similar reductions occur at $r = 0.4$ and $r = 0.8$. Therefore, the Hartmann number acts as a controlling damping parameter in both the transient and steady regimes.

This result is consistent with previous MHD flow studies, where increasing magnetic-field strength reduces the motion of conducting fluids through Lorentz-force damping [13], [15]. In the present annular configuration, the magnetic field reduces the entire velocity profile while preserving the no-slip condition at the boundaries.

4.3 Effect of time on inner-wall skin friction

Figure 4 shows the effect of time on the skin friction at the inner cylinder $r = \lambda$ for $M = 1.0$. The inner-wall skin friction is positive because the velocity increases from zero at the inner wall toward the interior of the annular gap. At early times, the developing velocity field produces a rapid variation in the wall gradient. As time increases, the skin friction approaches a limiting steady value.

Table 2 supports this behaviour. For $M = 1.0$ and $\lambda = 0.4$, the RSA value of the inner-wall skin friction is 0.3601 at $T = 0.2$, 0.3613 at $T = 0.4$, and 0.3612 at steady state. The small difference between the transient and steady values indicates that the wall shear approaches its steady limit as the flow becomes fully developed. Similar convergence is observed for $\lambda = 0.6$ and $\lambda = 0.8$.

The values also show that the skin friction decreases as λ increases. For $M = 1.0$ at steady state, the inner-wall skin friction decreases from 0.3612 at $\lambda = 0.4$ to 0.2190 at $\lambda = 0.6$, and then to 0.1038 at $\lambda = 0.8$. This indicates that the radius ratio strongly affects the wall-gradient distribution.

4.4 Effect of time on outer-wall skin friction

Figure 5 shows the effect of time on the skin friction at the outer cylinder $r = 1$ for $M = 1.0$. The skin friction at the outer wall is negative because the velocity decreases from the interior maximum to zero at the outer wall. Hence, the radial velocity gradient at $r = 1$ is negative under the adopted sign convention.

The numerical values in Table 2 confirm the convergence of outer-wall skin friction with time. For $M = 1.0$ and $\lambda = 0.4$, the RSA value changes from -0.2626 at $T = 0.2$ to -0.2634 at $T = 0.4$, and approaches the steady-state value -0.2632. The agreement between the transient and steady values improves at large time. This confirms that the Riemann-sum inversion recovers the expected steady wall-shear behaviour.

The magnitude of the outer-wall shear also decreases as λ increases. For $M = 1.0$ at steady state, the outer-wall skin friction changes from -0.2632 at $\lambda = 0.4$ to -0.1844 at $\lambda = 0.6$, and then to -0.0964 at $\lambda = 0.8$. The reduction in magnitude reflects the influence of annular geometry on the radial distribution of velocity gradients.

4.5 Effect of Hartmann number on inner-wall skin friction

Figure 6 presents the influence of the Hartmann number on the inner-wall skin friction for fixed $T = 0.02$. Increasing M reduces the inner-wall skin friction. This occurs because the magnetic field suppresses the axial velocity and weakens the velocity gradient transmitted to the wall.

Table 2 confirms this trend. At $T = 0.2$ and $\lambda = 0.4$, the RSA inner-wall skin friction decreases from 0.3686 for $M = 0.5$ to 0.3601 for $M = 1.0$. At steady state, the corresponding value decreases from 0.3699 to 0.3612. Similar reductions are observed at $\lambda = 0.6$ and $\lambda = 0.8$. Therefore, magnetic damping reduces not only the velocity magnitude but also the inner-wall shear.

4.6 Effect of Hartmann number on outer-wall skin friction

Figure 7 shows the effect of Hartmann number on the skin friction at the outer wall. Since the outer-wall derivative is negative, the effect of increasing M is interpreted in terms of the magnitude of the shear. The results show that increasing M reduces the magnitude of the outer-wall skin friction. For example, at $T = 0.2$ and $\lambda = 0.4$, Table 2 shows that the outer-wall RSA skin friction changes from -0.2681 for $M = 0.5$ to -0.2626 for $M = 1.0$. At steady state, the corresponding values are -0.2689 and -0.2632. Thus, the magnetic field weakens the wall shear by damping the flow field throughout the annulus.

This behaviour is physically consistent with the velocity results in Figure 3. Since the magnetic field reduces the axial velocity, the radial velocity gradient at the wall is also reduced in magnitude. The wall shear therefore reflects the same Lorentz-force damping mechanism observed in the velocity profiles.

4.7 Consistency of the semi-analytical solution

Tables 1 and 2 compare the transient RSA results with the steady-state values. For both velocity and skin friction, the RSA values approach the steady-state values as T increases. This agreement supports the consistency of the Laplace-transform solution and the numerical inversion procedure.

In Table 1, the RSA velocity values at $T = 10^4$ coincide with the steady-state values to the reported decimal places. In Table 2, the same agreement is observed for the skin-friction values at both annular walls. This confirms that the transient solution correctly recovers the steady-state behaviour at large time.

The results are therefore consistent with the mathematical structure of the governing problem: the pressure gradient drives the flow, viscosity distributes momentum across the annulus, and the magnetic field introduces a resistive force proportional to the velocity.

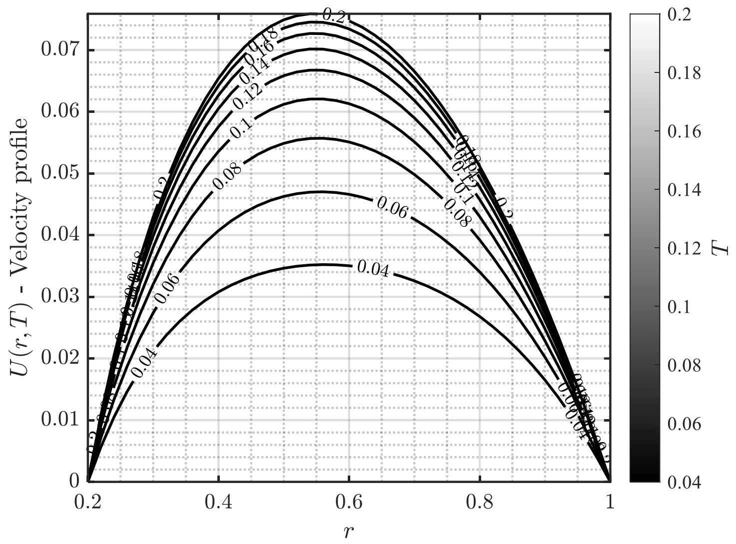

Figure 2: Effect of dimensionless time (T) on the velocity profile for $M = 1.0$.

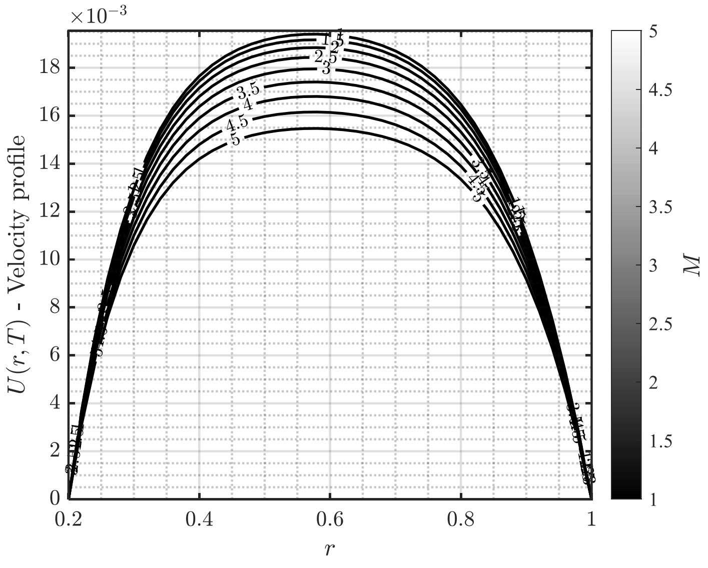

Figure 3: Effect of Hartmann number (M) on the velocity profile for fixed $T = 0.02$.

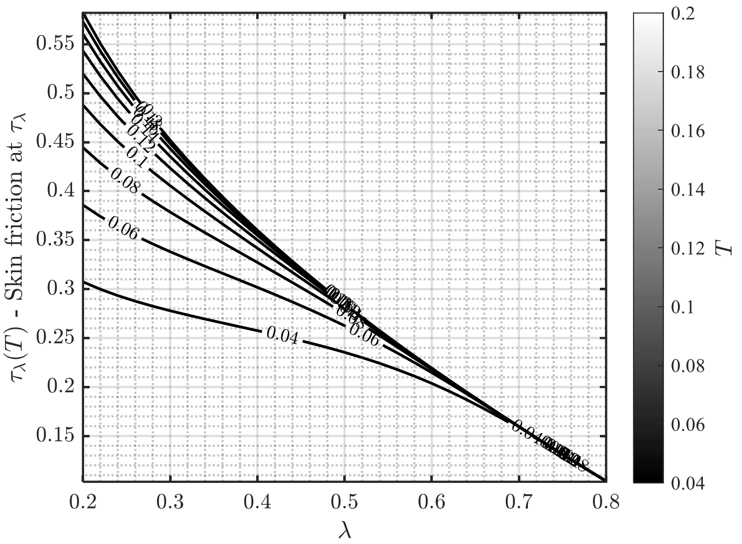

Figure 4: Effect of dimensionless time (T) on the skin friction at $r = \lambda$ for $M = 1.0$.

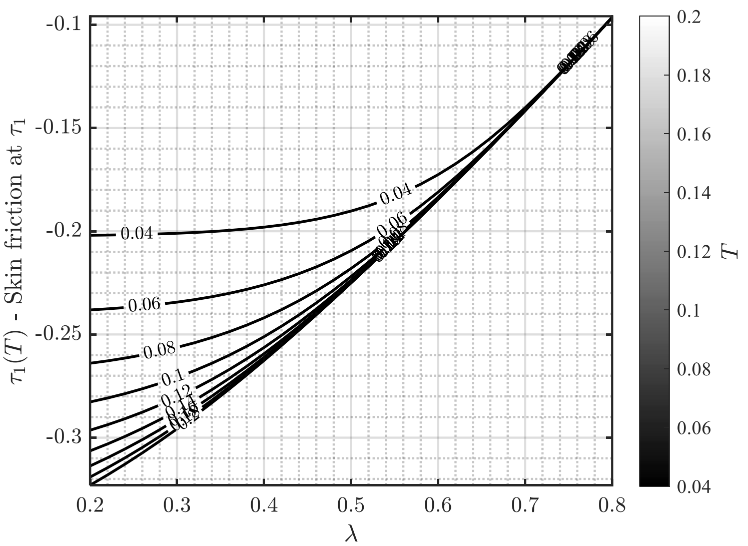

Figure 5: Effect of dimensionless time (T) on the skin friction at $r = 1$ for $M = 1.0$.

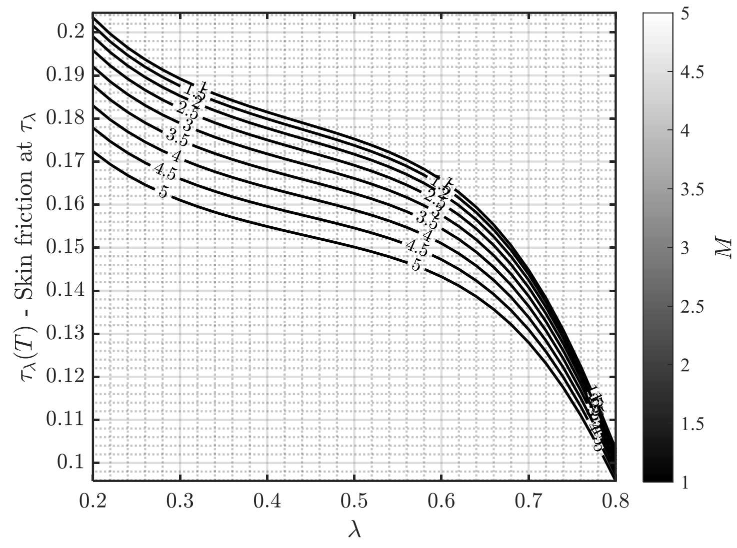

Figure 6: Effect of Hartmann number (M) on the skin friction at $r = \lambda$ for fixed $T = 0.02$.

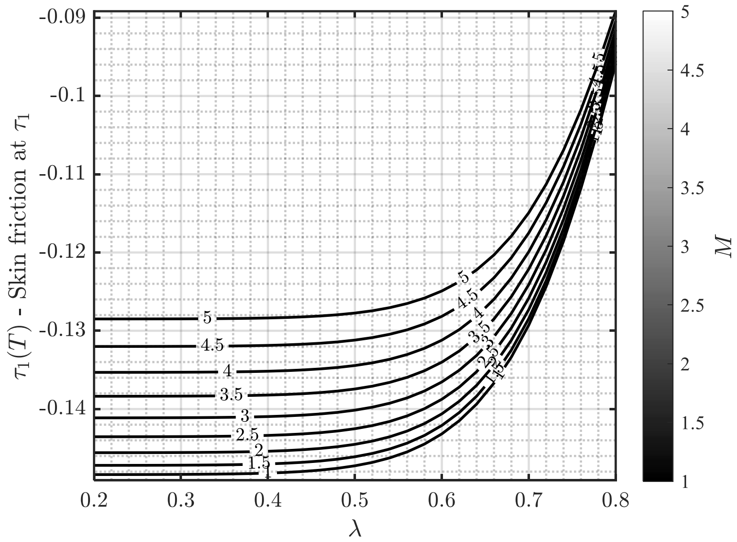

Figure 7: Effect of Hartmann number (M) on the skin friction at $r = 1$ for fixed $T = 0.02$.

Table 1: Numerical values of axial velocity profile for different values of T, and M.

Velocity profile					
		$M = 0.5$		$M = 1.0$	
T	r	RSA	Steady-state	RSA	Steady-state
0.2	0.4	0.0682	0.0721	0.0654	0.0685
	0.6	0.0780	0.0824	0.0747	0.0783
	0.8	0.0532	0.0558	0.0511	0.0533
0.4	0.4	0.0719	0.0721	0.0684	0.0685
	0.6	0.0822	0.0824	0.0782	0.0783
	0.8	0.0557	0.0558	0.0532	0.0533
	0.4	0.0721	0.0721	0.0685	0.0685

10^4	0.6 0.8	0.0824 0.0558	0.0824 0.0558	0.0783 0.0533	0.0783 0.0533

Table 2: Numerical values of the skin friction at $r = \lambda$ and $r = 1$ for different values of T, and M.

		Skin friction at $r = \lambda$				Skin friction at $r = 1$			
		$M = 0.5$		$M = 1.0$		$M = 0.5$		$M = 1.0$	
T	λ	RSA	Steady State	RSA	Steady State	RSA	Steady State	RSA	Steady State
0.2	0.4	0.3686	0.3699	0.3601	0.3612	-0.2681	-0.2689	-0.2626	-0.2632
	0.6	0.2214	0.2213	0.2191	0.2190	-0.1863	-0.1862	-0.1845	-0.1844
	0.8	0.1042	0.1041	0.1039	0.1038	-0.0967	-0.0966	-0.0965	-0.0964
0.4	0.4	0.3701	0.3699	0.3613	0.3612	-0.2690	-0.2689	-0.2634	-0.2632
	0.6	0.2214	0.2213	0.2191	0.2190	-0.1863	-0.1862	-0.1845	-0.1844
	0.8	0.1042	0.1041	0.1040	0.1038	-0.0967	-0.0966	-0.0965	-0.0964
10^4	0.4	0.3699	0.3699	0.3612	0.3612	-0.2689	-0.2689	-0.2632	-0.2632
	0.6	0.2213	0.2213	0.2190	0.2190	-0.1862	-0.1862	-0.1844	-0.1844
	0.8	0.1041	0.1041	0.1038	0.1038	-0.0966	-0.0966	-0.0964	-0.0964

5 Conclusion

A semi-analytical study has been presented for unsteady magnetohydrodynamic axial flow of an incompressible, viscous, electrically conducting Newtonian fluid through an annulus bounded by two stationary concentric cylinders. The flow is driven by a constant axial pressure gradient and subjected to a uniform transverse magnetic field. Under the low-magnetic-Reynolds-number approximation, the induced magnetic field is neglected and the magnetic effect is represented by a Lorentz-force damping term.

The governing momentum equation was non-dimensionalized using the outer-cylinder radius, viscous time scale, and pressure-gradient velocity scale. The resulting transient boundary-value problem was solved using the Laplace transform method. Because the transformed solution involves modified Bessel functions with complex arguments, the Riemann-sum approximation was used to recover the time-dependent velocity and skin-friction fields. Steady-state expressions were also obtained for comparison with the large-time solution. The main findings are as follows:

1. The axial velocity develops from the initial rest condition and approaches a steady-state annular profile as time increases.
2. The maximum velocity occurs within the annular gap, while the velocity satisfies the no-slip condition at both cylinder walls.

3. Increasing the Hartmann number reduces the axial velocity because the Lorentz force opposes the motion of the conducting fluid.
4. The inner-wall skin friction is positive, while the outer-wall skin friction is negative under the derivative convention $C_f = \partial V / \partial r$.
5. The magnitude of the skin friction at both walls decreases as the Hartmann number increases.
6. The radius ratio affects the wall shear stress by modifying the annular gap and the radial distribution of the velocity gradient.
7. The transient RSA results approach the steady-state values at large time, confirming the consistency of the semi-analytical solution.

The study provides a compact semi-analytical description of MHD start-up flow in an annular passage. The results may serve as reference solutions for idealized hydromagnetic annular-flow problems.

Conflict of Interest: The authors declare that they have no known competing financial interests or personal relationships that could have appeared to influence the work reported in this manuscript.

References

[1] B. K. Jha and Y. J. Danjuma, "Transient Dean flow in a channel with suction/injection: A semi-analytical approach," *Proceedings of the Institution of Mechanical Engineers, Part E: Journal of Process Mechanical Engineering*, vol. 233, no. 5, pp. 1036–1044, 2019, doi: 10.1177/0954408919825718.

[2] B. K. Jha and J. D. Yahaya, "Transient Dean flow in an annulus: a semi-analytical approach," *Journal of Taibah University for Science*, vol. 13, no. 1, pp. 169–176, 2018, doi: 10.1080/16583655.2018.1549529.

[3] Y. J. Danjuma, *Transient Flow Formation inside an Annulus: A Semi-Analytical Approach*. DE, 2019. [Online]. Available: https://www.morebooks.de/store/gb/book/transient-flow-formation-inside-an-annulus:-a-semi-analytical-approach/isbn/978-620-0-23920-4

[4] B. K. Jha and Y. J. Danjuma, "Transient generalized Taylor-Couette flow: a semi-analytical approach," *Journal of Taibah University for Science*, vol. 14, no. 1, pp. 445–453, 2020, doi: 10.1080/16583655.2020.1745477.

[5] S. T. Wereley and R. M. Lueptow, “Velocity field for Taylor–Couette flow with an axial flow,” *Physics of Fluids*, vol. 11, no. 12, pp. 3637–3648, 1999.

[6] R. M. Lueptow, A. Docter, and K. Min, “Stability of axial flow in an annulus with a rotating inner cylinder,” *Physics of Fluids A*, vol. 4, no. 11, pp. 2446–2558, 1992.

[7] U. K. Sarkar and N. Biswas, “Exact and limiting solutions of fluid flow for axially oscillating cylindrical pipe and annulus,” *SN Appl. Sci.*, vol. 3, no. 3, p. 339, 2021.

[8] G. Ali, M Ahmad, F. Ali, & A. Khan. Couette flow of viscoelastic dusty fluid through a porous oscillating plate in a rotating frame along with heat transfer. *Heat Transfer, 53*(8), 4588–4607. 2024, https://doi.org/10.1002/htj.23127

[9] Y. Zhang, & C. Liu. Unsteady magnetohydrodynamic oblique stagnation point slip flow of Maxwell fluid over an oscillating–stretching cylinder with Cattaneo–Christov double diffusion model. *Numerical Heat Transfer, Part B: Fundamentals, 86*(9), 3018–3038. 2024 https://doi.org/10.1080/10407790.2024.2352854

[10] T. Hayat, S. Qayyum, M. Imtiaz, and A. Alsaedi (2016). Magnetohydrodynamic (MHD) flow of Jeffrey fluid over a stretching cylinder with slip conditions and heat transfer. *Journal of Molecular Liquids, 220*, 846–854. https://doi.org/10.1016/j.molliq.2016.04.083

[11] S. Aberkane, M. Ihdene, M. Moderes, and A. Ghezal, “Axial magnetic field effect on Taylor-Couette flow,” *Journal of applied fluid mechanics*, vol. 8, no. 2, pp. 255–264, 2014.

[12] P. Dash, N. B. Barik, and K. L. Ojha. Effect of sinusoidal pressure gradient on MHD flow of viscoelastic fluid in a channel. *Numerical Heat Transfer, Part B: Fundamentals, 86*(4), 827–839. 2023, https://doi.org/10.1080/10407790.2023.2296093

[13] O. D. Makinde and T. Chinyoka, “MHD transient flows and heat transfer of dusty fluid in a channel with variable physical properties and Navier slip condition,” *Computers and Mathematics with Applications*, vol. 60, no. 3, pp. 660–669, 2010, doi: 10.1016/j.camwa.2010.05.014.

[14] T. Gul, M. Jan, Z. Shah, S. Islam, and M. A. Khan, “Unsteady Transient Couette and Poiseuille Flow Under The effect Of Magneto-hydrodynamics and Temperature,” *J. Appl. Environ. Biol. Sci*, vol. 5, no. 7, pp. 339–353, 2015.

[15] A. Kumar and A. Singh, "Transient magnetohydrodynamic Couette flow with ramped velocity," *International Journal of Fluid Mechanics Research*, vol. 37, no. 5, 2010.

[16] J. P. Maurya, S. Lal Yadav, and A. K. Singh, "Analysis of magnetohydrodynamics transient flow in a horizontal annular duct," *Int. J. Dyn. Control*, vol. 4, 2020, doi: 10.1007/s40435-020-00611-4.

[17] B. K. Jha and Y. J. Danjuma, "Transient generalized Taylor–Couette flow of a dusty fluid: A semi-analytical approach," *Partial Differential Equations in Applied Mathematics*, vol. 5, p. 100400, 2022.

[18] B. K. Jha and Y. J. Danjuma, "Unsteady Dean flow formation in an annulus with partial slippage: A riemann-sum approximation approach," *Results in Engineering*, vol. 5, p. 100078, Mar. 2020, doi: 10.1016/j.rineng.2019.100078.